A parameterization of cirrus cloud formation: Homogeneous freezing of supercooled aerosols

B. Kärcher

Deutsches Zentrum für Luft- und Raumfahrt, Institut für Physik der Atmosphäre, Oberpfaffenhofen, Germany

U. Lohmann

Atmospheric Science Program, Department of Physics, Dalhousie University, Halifax, Nova Scotia, Canada

Received 26 January 2001; revised 12 June 2001; accepted 8 August 2001; published 17 January 2002.

[1] The nucleation and initial growth of ice crystals in cirrus clouds at low (<235 K) temperatures prevailing in the upper troposphere and in the tropopause region is theoretically considered. The analysis explains the dependence of the number density of ice crystals on the vertical velocity and temperature seen in numerical simulations of cirrus formation when the timescale of depositional growth of the pristine ice particles is fast compared to the timescale of the freezing event. In such cases, applicable in many situations, the number of crystals formed via homogeneous freezing of aqueous solution droplets is rather insensitive to details of the aerosol size distribution, but increases rapidly with updraft velocity and decreases with temperature. The derived parameterization is validated with parcel model simulations, and its applicability for use in climate models is discussed. The potential role of aerosol size and heterogeneous freezing processes in altering the predicted cirrus properties is briefly addressed. *INDEX TERMS:* 0305 Atmospheric Composition and Structure: Aerosols and particles (0345, 4801), 0320 Atmospheric Composition and Structure: Cloud physics and chemistry, 0365 Atmospheric Composition and Structure: Troposphere–composition and chemistry, 0399 Atmospheric Composition and Structure: General or miscellaneous; *KEYWORDS:* aerosol, cirrus cloud, climate model, parameterization

1. Introduction

[2] The largest uncertainties in the prediction of climate forcing from anthropogenic changes in atmospheric composition arise from attempts to quantify the climatic effects of aerosols on clouds in global climate models [*Intergovernmental Panel on Climate Change*, 2001]. An important component of this uncertainty is related to the indirect forcing, associated with the link between aerosol properties such as particle number and size, chemical composition, and ability to act as cloud condensation nuclei (CCN) [*Charlson and Heintzenberg*, 1995]. The latter influences cloud properties such as droplet number and size, albedo, precipitation rate, and lifetime [*Charlson et al.*, 1987; *Albrecht*, 1989; *Twomey*, 1992].

[3] Quantifying the relationship between aerosol and cloud properties is a challenging enterprise. Considerable progress has been made in representing the indirect effect of aerosols on warm clouds (consisting of water droplets), either by developing empirical relationships between aerosol mass and cloud droplet number [*Boucher and Lohmann*, 1995] or by deriving approximate analytic expressions to calculate the fraction of particles acting as CCN in a given ensemble of aerosols [*Ghan et al.*, 1997; *Abdul-Razzak et al.*, 1998].

[4] In contrast, very little information is available concerning the interaction of aerosols and cold cirrus clouds (consisting of ice crystals), despite the fact that cirrus clouds exert a significant potential climatic impact [*Liou*, 1986]. State-of-the-art general circulation models (GCMs) represent cirrus clouds either by diagnosing the ice water portion from the predicted total water content as a function of temperature [*Del Genio et al.*, 1996] or by separately predicting cloud ice mixing ratio [e.g., *Fowler et al.*, 1996]. All of these schemes apply the saturation adjustment scheme for condensation and deposition; that is, no supersaturation with respect to ice is allowed. Only recently, *Wilson and Ballard* [1999] introduced an ice phase scheme into the U.K. Meteorological Office Unified Model that allows subsaturation or supersaturation with respect to ice by explicitly solving the growth equation for a single ice particle.

[5] Several studies have estimated the indirect effect of anthropogenic aerosols by conducting numerical experiments with preindustrial and present-day emissions [e.g., *Rotstayn*, 1999; *Lohmann et al.*, 2000]. These studies consider both the effect of increasing cloud albedo due to more but smaller cloud droplets for a given liquid water path and the increase in cloud lifetime due to the reduced precipitation efficiency. Whereas *Rotstayn* [1999] used an empirical relationship between sulfate aerosol mass and cloud droplet number, *Lohmann et al.* [2000] predicted cloud droplet number concentration and parameterized cloud droplet nucleation for an internally as well as an externally mixed aerosol. The estimates for both indirect aerosol effects in these studies range from -1.1 to -2.1 W m^{-2}. In these models the changes in anthropogenic aerosol concentration have no direct impact on ice clouds. The only link to ice clouds is heterogeneous freezing of cloud droplets. The change in longwave radiation in these simulations only amounted to $0.1-0.2$ W m^{-2}.

[6] Ice nucleation is a fundamental cloud process. The processes involved in ice formation in cirrus clouds seem to be largely understood only in the case of homogeneous freezing of supercooled droplets. In contrast, knowledge about ice formation caused by heterogeneous freezing nuclei (FN) at low temperatures are poorly understood. This is partly caused by the lack of information about the origin, spatial distribution, and chemical nature of the FN. Throughout this work, we define FN as ice-nucleating aerosols. FN may not necessarily be very

0148-0227/02/2001JD000470$09.00

efficient ice nuclei (particles that already form ice at a few percent supersaturation with respect to ice or at rather warm temperatures.)

[7] The importance of homogeneous freezing of supercooled aerosols to cirrus cloud formation under upper tropospheric conditions has been emphasized in numerous previous studies, dating back to the late 1980s [e.g., *Heymsfield and Sabin*, 1989; *Sassen and Dodd*, 1989]. The apparent lack of efficient FN, the large number of small ice crystals measured in young cirrus, and the high relative humidities observed frequently [e.g., *Newell et al.*, 1996; *Schumann et al.*, 2000; *Jensen et al.*, 2001] render homogeneous freezing an important cloud formation mechanism. While the occurrence of heterogeneous freezing processes in cold cirrus has been inferred from case studies, the role of heterogeneous FN in cirrus formation is not fully understood [e.g., *DeMott et al.*, 1997]. It seems likely that wave-generated cirrus clouds form predominantly at large supersaturations with respect to ice and that direct deposition of water vapor onto heterogeneous FN is an insignificant process [*Heymsfield and Miloshevich*, 1995].

[8] First attempts to investigate the importance of contact nucleation on climate were carried out by *Lohmann* [2001]. Contact nuclei are a subset of FN; contact freezing is important in the formation of ice in mixed phase clouds at temperatures above 235 K. If dust aerosols acting as contact nuclei are assumed to lose their nucleability by forming an internally mixed aerosol with sulfate, then contact nucleation is partly inhibited. On the other hand, if all contact nuclei are assumed to be insoluble carbonaceous aerosols, as found in contrails and some cirrus clouds [*Ström and Ohlsson*, 1998], then contact nucleation is more important. This has implications for the ice water path and cloud radiative forcing.

[9] In the context of climate modeling, it is highly desirable to have accurate scaling models for the attainable cirrus parameters, such as the total crystal number and mean particle size in newly formed cirrus. Previous work on cirrus cloud parameterization by homogeneous freezing has been mostly based on the derivation of modified classical nucleation rate expressions, containing dependences on temperature and solute concentrations in aqueous solutions (ammoniated sulfates and sulfuric acid), or on an effective freezing temperature that is proportional to the freezing point depression caused by the presence of solute in the aerosol [e.g., *DeMott et al.*, 1998; *Khvorostyanov and Sassen*, 1998; *Tabazadeh et al.*, 2000]. However, with the exception of the relationships provided by *Sassen and Benson* [2000], these parameterizations neither predict the number of ice crystals nucleated after a given time nor include the explicit dependence on the cloud forcing mechanism.

[10] Our primary goal is to develop a detailed theoretical understanding of the controlling physics of homogeneous freezing in cirrus clouds (at temperatures T below ~235 K or at altitudes above 8 km and pressures p below 350 hPa) based on recent experimental data summarized by *Koop et al.* [2000]. Because the direct application of size-resolved cirrus microphysical models to GCMs is impractical due to the large demand of additional computation time, we develop a parameterization that expresses the properties of young cirrus clouds in terms of variables that influence ice formation most significantly and that are also carried in a GCM. As we will show in this work, these variables appear to be the updraft velocity of the air mass within which freezing occurs, the temperature, and aerosol properties that determine the threshold relative humidity critical for freezing. The new parameterization proposed here applies to a wide class of aqueous solutions relevant to homogeneous freezing in the atmosphere. A treatment of heterogeneous freezing processes is beyond the scope of this work but will be considered as an extension of the present model framework in the future.

[11] The theoretical model of ice nucleation and growth in young cirrus is outlined in detail in section 2. In section 3 it is validated by numerical simulations of the cloud formation process using an adiabatic parcel model, and the main results are compared to observations. Section 4 discusses aspects of applying the new parameterization in a large-scale atmospheric model. Section 5 discusses potential changes of the cloud parameterization when aerosol size effects and heterogeneous FN are taken into account. Section 6 summarizes the main results of this work and highlights future research needs.

2. Theoretical Model of Ice Nucleation and Growth

[12] This section provides the physical basis and theoretical description of the cirrus cloud initiation process in an adiabatically rising air parcel.

2.1. Basic Relations and Solution Strategy

[13] Our starting point is the definition of the ice saturation ratio $S_i = p_w/p_{sat}(T)$, where p_w is the partial pressure of water vapor (H_2O) and $p_{sat}(T)$ is the H_2O saturation vapor pressure over a plane ice surface, taken from *Hanson and Mauersberger* [1988]. Consistent with p_{sat}, we consider the Clausius-Clapeyron equation $d\ln(p_{sat})/d\ln(T) = L_s M_w/(RT)$, with the latent heat of sublimation $L_s = 2.836 \times 10^6$ J kg^{-1}, the molecular mass of water $M_w = 18 \times 10^{-3}$ kg mol^{-1}, and the universal gas constant $R = 8.314$ J (mol K)$^{-1}$. Finally, the adiabatic cooling rate $dT/dt = -gw/c_p$ connects the temperature change in the air parcel to the vertical velocity w, the acceleration of gravity $g = 9.81$ m s^{-2}, and the specific heat capacity of air $c_p = 1005$ J (kg K)$^{-1}$. Throughout this work, we assume that w is constant.

[14] Differentiation of S_i with respect to time t leads to the central equation [*Pruppacher and Klett*, 1997]

$$\frac{dS_i}{dt} = a_1 S_i w - (a_2 + a_3 S_i) R_i, \tag{1}$$

where $a_1 = L_s M_w g/(c_p RT^2) - Mg/(RT)$, with the molecular mass of air $M = 29 \times 10^{-3}$ kg mol^{-1}; $a_2 = 1/n_{sat}$, the inverse H_2O number density at ice saturation; $a_3 = L_s^2 M_w m_w/(c_p pTM)$, with the mass of a water molecule $m_w = 3 \times 10^{-26}$ kg; and the freezing/growth term

$$R_i = \frac{\rho_i}{m_w} \int_{-\infty}^{t} dt_0 \dot{n}_i(t_0) 4\pi r_i^2(t_0, t) \frac{dr_i}{dt}(t_0, t), \tag{2a}$$

with the ice particle mass density $\rho_i \simeq 0.925 \times 10^3$ kg m^{-3}. In the integrand, $\dot{n}_i(t_0)dt_0$ denotes the number density of aerosol particles that freeze within the time interval between t_0 and $(t_0 + dt_0)$, $r_i(t_0,t)$ is the radius of the ice particle at time t that froze and commenced to grow at time $t_0 < t$, and dr_i/dt is the radial growth rate of that ice particle. Thus R_i describes the rate of depletion of water vapor by the growing ice particles as a function of time. The function $\dot{n}_i$ is related to the freezing nucleation rate J via

$$\dot{n}_i = \frac{4\pi}{3} r_0^3 n J, \tag{2b}$$

where $r_0 = r_i(t_0)$ and n describe the aerosol particle radius and number density prior to the freezing event and J denotes the nucleation rate per unit time per unit volume of aerosol. At this point, we are free to choose any nucleation rate that serves to describe ice formation in atmospheric aerosols. Note that as both dr_i/dt and J depend on S_i, (1) is actually a highly nonlinear integro-differential equation. In noting (2a) and (2b), we implicitly assume the aerosol particles to be monodisperse; this could be generalized to include an aerosol size spectrum by introducing a radial distribution dn/dr_0 that replaces n and integrating over r_0. However, as we shall demonstrate in section

3.2, this generalization does not need to be considered in the present work.

[15] In applying (1) to the activation of CCN into water droplets, the saturation ratio, appearing explicitly in the terms on the right-hand side, is usually approximated by unity, because water saturation is exceeded only slightly in the atmosphere (a few percent at most). In contrast, homogeneous ice nucleation requires large saturation ratios over ice (1.4–1.7 in the temperature range 235–195 K) [e.g., *Tabazadeh et al.*, 2000; *Koop et al.*, 2000], and even heterogeneous nuclei such as soot particles coated with water and sulfuric acid may require substantial ($S_i \simeq 1.3$ or higher) supersaturations before freezing occurs [e.g., *Kärcher et al.*, 1998; *DeMott et al.*, 1999]. Therefore we do not introduce this approximation for S_i in (1).

[16] An inspection of (1) reveals that S_i first increases upon cooling (described by the first term on the right-hand side). At some critical value S_{cr}, freezing produces the first ice particles. When a sufficiently large number of crystals are formed, they start depleting the existing water vapor (described by the second term on the right-hand side). At this point, S_i reaches its peak value. The competition between generating supersaturation by updraft and cooling and removing supersaturation by depositional growth of the ice crystals eventually determines the microphysical properties of the developing young cirrus cloud. When S_i drops below S_{cr}, nucleation stops, and the H_2O number density decreases rapidly. Eventually, S_i approaches a steady state value. This general behavior of S_i is schematically depicted in Figure 1. Cases where the aerosol particles become activated to nearly pure water droplets prior to freezing, which may occur at high updraft speeds and at relatively warm temperatures above 235 K, are not considered in this work.

[17] As suggested by *Twomey* [1959], an approximate analytical solution of (1) is obtained by identifying the conditions (hereinafter marked with an asterisk) where the saturation ratio reaches a maximum, rather than by solving the model equations exactly. Expressed differently, the condition

$$\frac{a_1 \cdot S_i^*}{a_2^* + a_3^* S_i^*} w = R_i^* \tag{3}$$

will lead us to an analytic expression for the number density of ice crystals n_i after the freezing event. We expect that this solution strategy results in a good approximation of n_i, because freezing takes place only in a short time interval where S_i lies between S_{cr} and S_{i*} or in the region between the two horizontal dashed lines in Figure 1.

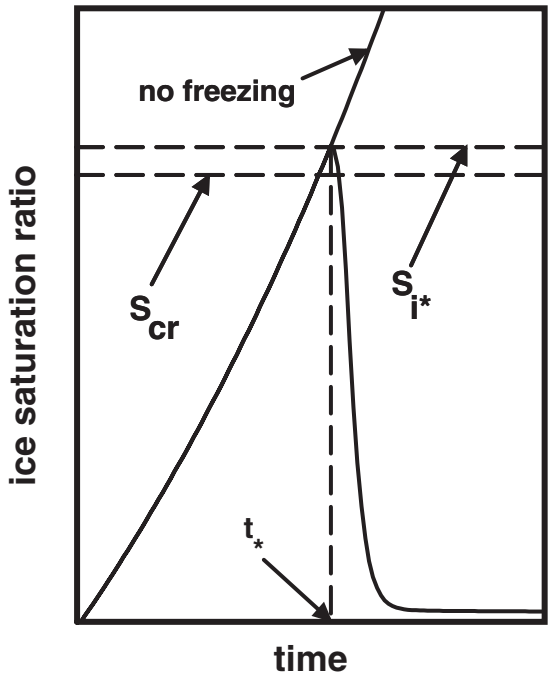

Figure 1. Temporal evolution of the ice saturation ratio in a uniform vertical ascent. Curve labeled "no freezing" neglects ice particle formation, in which case S_i grows exponentially in the rising air parcel. If ice particles form and grow above a critical value S_{cr}, the saturation ratio reaches a maximum value S_{i*} and falls off rapidly due to depletion of the available water vapor. If the air parcel continues to rise after S_i passes its maximum, S_{i*} may exceed S_{cr} by several percent, and S_i approaches a limiting value slightly above unity; otherwise, S_{i*} is approximately equal to S_{cr}, and S_i relaxes to unity. According to numerical simulations, the difference between S_{i*} and S_{cr} is much smaller than the threshold saturation ratio S_{cr}, and the relaxation time is much smaller than t_*.

2.2. Freezing Nucleation Rates

[18] The rate J to be used in (2b) will generally depend on the chemical composition of the aerosol particles. A critical nucleation rate J_{cr} may be defined that is sufficiently large to allow rapid formation of ice in the atmosphere. For example, we may choose J_{cr} such that a particle with radius $r_0 = 0.25$ μm (a typical size of a freezing aerosol particle) freezes within $\Delta t = 20$ min (a typical time step in GCMs), leading to $J_{cr} = 3\,(4\pi\, r_0^3\, \Delta\, t)^{-1} \simeq 10^{10}$ cm^{-3} s^{-1}. The parameterization derived below is not very sensitive to this value.

[19] Homogeneous freezing of liquid, supercooled aerosol particles, consisting of water and acidic components, is an important ice formation mechanism under upper tropospheric conditions. The exception would be a slowly rising air mass with more than normal heterogeneous FN with more facile freezing properties. Here we apply the homogeneous freezing formulation for chemically uniform aerosols developed by *Koop et al.* [2000] from a series of laboratory studies. The temperature-dependent, critical saturation values S_{cr} were measured for a variety of supercooled aqueous solution droplets, including the atmospherically relevant sulfuric acid, ammoniated sulfate, and ternary sulfuric acid/nitric acid solutions. Surprisingly, the dependences of S_{cr} on T are similar for all aerosol types investigated within experimental uncertainties; that is, they are independent of the chemical nature of the solutes. This enabled *Koop et al.* [2000] to present a unified description of homogeneous freezing, where the nucleation rate J depends only on the water activity, or equivalently on S_i, and on T. (The water activity is essentially equal to the relative humidity, because atmospheric aerosols are in most cases in local equilibrium with water below water saturation. The largest aerosol particles may not reach equilibrium at low temperatures and in strong updrafts due to diffusive limitations of the water uptake rate.)

[20] We note two expressions related to J that we employ in section 2.3. First, we have derived the critical values S_{cr} at each temperature by varying S_i until $J = J_{cr} = 10^{10}$ cm^{-3} s^{-1} for a 0.25 μm particle. The numerical fit reads

$$S_{cr} = 2.583 - \frac{T\,[K]}{207.83}. \tag{4}$$

Next, we computed the derivative of $\ln(J)$ with respect to T at the critical saturation S_{cr} numerically and fitted the results, leading to

$$\left(\frac{\partial \ln(J)}{\partial T}\right)_{S_i = S_{cr}} \left[\frac{1}{\mathrm{K}}\right] = 4.37 - 0.03\,T\,[K]. \tag{5}$$

[21] Equations (4) and (5) are valid for freezing temperatures between ~190 and ~240 K. We do not take into account the small dependence of S_{cr} on the particle size, which enters S_{cr} through the

dependence of J_{cr} on r_0; see above. The laboratory measurements indicate that, for example at 220 K, S_{cr} increases from 1.50 to 1.52 when r_0 decreases from 1 to 0.1 μm. Such small changes are within the spread of S_{cr} measured for different aerosol types at constant values of T and r_0.

2.3. Analytical Solution

[22] A key element of the solution procedure is to find an accurate solution of (2a). To compute R_i, we follow *Ford* [1998], who applied a similar model framework to describe ice nucleation in aircraft contrails. However, we cannot employ his solution method directly, because several fundamental differences exist between contrail and cirrus formation: (1) Contrails form in isobarically cooling air parcels, forced by turbulent mixing between the warm, moist exhaust air and the colder, drier ambient air. In most cases, cirrus clouds form in adiabatically rising air parcels. (2) Ice crystals in contrails form by activation of particles into liquid water droplets, which then freeze to form ice crystals. Hygroscopic aerosol particles usually freeze to form cirrus ice crystals without passing a water activation state. (3) Point (2) implies that different freezing mechanisms are acting in contrails and cirrus clouds (freezing of water droplets versus freezing of acidic aerosol droplets), presumably with different nucleation rates.

[23] To solve (2a), we first assume an approximate functional dependence of $\dot{n}_i(t_0)$, which is a priori unknown. Fortunately, the main contribution to R_i comes from times close to t_0, so that the specific temporal dependence is not crucial. As proposed by *Ford* [1998], we choose the analytically convenient form

$$\dot{n}_i(t_0) = \dot{n}_i(t)\exp[-(t - t_0)/\tau], \tag{6a}$$

where τ is the characteristic timescale for the nucleation event. By definition, the number of ice crystals present at time t is given by

$$n_i(t) = \int_{-\infty}^{t} dt_0 \dot{n}_i(t_0) = \dot{n}_i(t)\tau. \tag{6b}$$

We relate τ to the cooling rate of the air parcel by defining

$$\tau^{-1} = c\left(\left|\frac{\partial \ln(J)}{\partial T}\right|\right)_{S_i = S_{cr}} \frac{dT}{dt}, \tag{6c}$$

where the partial derivative is taken at the freezing threshold. In this definition of τ as the natural choice given the exponential approximation (6a), the unknown fit parameter c must be constrained by comparison with numerical simulations. It is not a unique function, but depends on the simulation model used, as different model formulations could lead to differences in the prediction of the cirrus initiation processes. The result obtained by comparison with our numerical calculations (see Section 3.2.1.) is given by

$$c(T) = \begin{cases} 100(22.6 - 0.1T[\mathrm{K}]) & T < 216\,\mathrm{K} \\ 100 & T \geq 216\,\mathrm{K}. \end{cases} \tag{6d}$$

[24] Next we provide the depositional growth law dr_i/dt for the ice crystals in (2a). An appropriate equation for diffusional growth, taking into account the effect of gas kinetics on the diffusional flux of H_2O molecules to the ice particles, is given by

$$\frac{dr_i}{dt} = \frac{m_w}{\rho_i}\frac{\alpha v_{th}}{4}\frac{n_{sat}(S_i - 1)}{1 + \frac{\alpha v_{th} r_i}{4D}} = \frac{b_1}{1 + b_2 r_i}, \tag{7}$$

where α is the deposition coefficient for H_2O molecules condensing on an ice surface, v_{th} is their thermal speed, and $D(T,p)$ is their diffusion coefficent in air [*Pruppacher and Klett*, 1997; chapter 13]. To simplify the notation, we introduce the variables b_1 and b_2. We use $\alpha = 0.5$, assume the ice particles to be spherical, and do not introduce a shape factor in (7).

[25] We inspect two limiting cases of (2a): for small values of $(t-t_0)$ (superscript 0), where $r_i^0 \gtrsim r_0$ and for large values of $(t-t_0)$superscript ∞, where $r_i^\infty \gg r_0$ or $b_2 r_i^\infty \gg 1$. Keeping in mind that the ice crystals are only formed near S_{cr}, we integrate (7) between t_0 and t for constant S_i and find

$$\frac{dr_i^0}{dt} = \frac{b_1}{1 + b_2 r_0}, \quad r_i^0(t_0, t) = r_0 + \frac{b_1(t - t_0)}{1 + b_2 r_0} \tag{8a}$$

$$\frac{dr_i^\infty}{dt} = \frac{b_1}{b_2 r_i^\infty}, \quad r_i^\infty(t_0, t) = \sqrt{\frac{2b_1(t - t_0)}{b_2}}. \tag{8b}$$

Inserting these solutions together with (6a) into (2a) and integrating from t_0 to t, we compute

$$R_i^0(t) = \frac{4\pi\rho_i}{m_w}\tau\dot{n}_i(t)\frac{b_1 r_0^2}{1 + b_2 r_0}[1 + 2\kappa(1 + \kappa)] \tag{9a}$$

$$R_i^\infty(t) = \frac{\rho_i}{m_w}\dot{n}_i(t)\left(2\pi\tau\frac{b_1}{b_2}\right)^{3/2}. \tag{9b}$$

In (9a) the parameter κ is defined as

$$\kappa = \tau\frac{b_1/r_0}{1 + b_2 r_0} \tag{10}$$

and is equal to the ratio of timescales for freezing (τ from (6c)) and initial growth ($r_0/(dr_i^0/dt)$ from (8a)). The solution labeled with 0 holds for $\kappa < 1$, while the solution labeled with ∞ is achieved for $\kappa > 1$.

[26] Figure 2 displays the curve $\kappa = 1$, discriminating between the fast-growth solution (9b) and the slow-growth solution (9a), in the parameter region of interest for $r_0 = 0.25$ μm. When the fast-growth solution applies, the growing ice particles rapidly lose their memory about the initial conditions, expressed by the fact that (9b) no longer depends on r_0, the size of the aerosol particles before

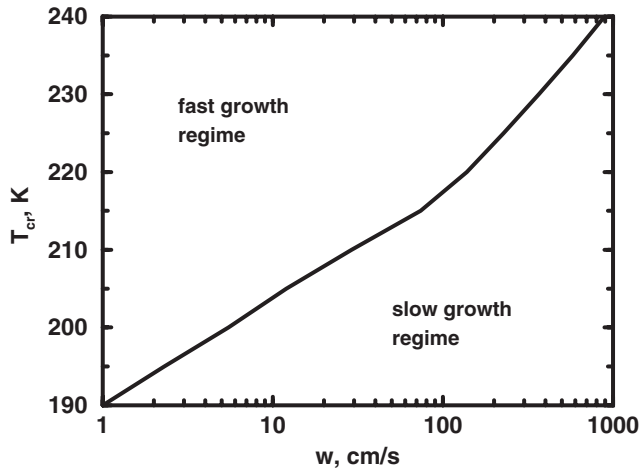

Figure 2. Fast-growth solution versus slow-growth solution. Solid curve connects the values of vertical velocity and freezing temperature for which the timescales of the freezing event and the initial growth of the ice crystals are identical. Along this curve the freezing/growth parameter κ, evaluated for an initial particle radius of 0.25 μm, equals unity. Regions above (below) the curve indicate combinations of w and T_{cr} where growth is fast (slow) compared to freezing.

freezing occurs. This implies that the number of ice crystals nucleated would be insensitive to the detailed shape of the aerosol size distribution, if we assumed one. In contrast, the solutions do depend on r_0 (and perhaps on the shape of the aerosol spectrum), when the slow-growth solution applies, where freezing occurs in a burst.

[27] As we will discuss in more detail in section 3.2.2., many relevant cases describing homogeneous cirrus formation in the atmosphere can be described by the fast-growth solution. As a first step in the development of a more universal parameterization scheme, we therefore concentrate on (9b) in the subsequent calculations and ignore the slow-growth case.

[28] We obtain the number of ice crystals n_{i*} at the point where S_i reaches a peak by setting (9b) equal to (3) and using (6b):

$$n_i = \frac{m_w}{\rho_i}\left(\frac{b_2}{2\pi b_1}\right)^{3/2}\frac{a_1 S_{cr}}{a_2 + a_3 S_{cr}}\frac{w}{\sqrt{\tau}}, \tag{11a}$$

where we have dropped the asterisks and the superscript ∞, for convenience. As an important step, we have set $S_{i*} = S_{cr}$. This is justified, because the peak saturation ratio will be close to the critical saturation ratio, except in strong updrafts at low temperatures; recall the discussion of Figure 1. Note again that the temperature used to evaluate the crystal concentrations must be the temperature T_{cr} at which S_{cr} is reached or surpassed in the rising air parcel. While these expressions do not explicitly depend on the total number of aerosol particles n, (11a) holds only as long as the calculated number of crystals does not exceed n. In other terms, (11a) must be constrained by n as an upper bound.

[29] The estimate for the mean ice particle radius at time $t = t_*$ is obtained from the defining equation

$$r_{i*} = 1\dot{n}_{i*}\tau_* \int_{-\infty}^{t_*} dt_0 r_i^{\infty}(t_0, t_*)\dot{n}_i(t_0);$$

on substituting (8b) and performing the integration

$$r_{i*} = \sqrt{\frac{\pi}{2}\frac{b_1}{b_2}}\tau. \tag{11b}$$

The cloud ice water mass, computed from $m_{i*} = 4\pi\rho_i n_{i*} r_{i*}^3/3$, takes the simple form

$$m_{i*} = \frac{\pi}{6} m_w \frac{a_1 S_{cr}}{a_2 + a_3 S_{cr}} w\tau. \tag{11c}$$

Equations (11b) and (11c) have a drawback: while nucleation ceases as soon as S_i falls below S_{cr}, the ice particles continue to grow as long as the air parcel is supersaturated, implying that (11c) seriously underestimates the real particle water content. To find a reasonable approximation for the total ice water mass, we add a second term to m_{i*} which takes this later growth phase into account until the saturation relaxes to unity:

$$m_i = \frac{\pi}{6} m_w \frac{a_1 S_{cr}}{a_2 + a_3 S_{cr}} w\tau + m_w n_{sat}(S_{cr} - 1). \tag{12a}$$

The corresponding final mean ice particle radius then follows from

$$r_i = \left(\frac{3m_i}{4\pi\rho_i n_i}\right)^{1/3}, \tag{12b}$$

with m_i from (12a). We note that the total ice water mass is dominated by the second term on the right hand side of (12a). It is clear that both r_i and m_i are lower limits in an air parcel that continues to rise after the freezing event, in which case a complete relaxation of the initial supersaturation is not achieved.

3. Discussion and Comparison With Simulations and Observations

[30] The aim of this section is to discuss the analytic results and to verify the theoretical model by a comparison with results obtained from a detailed numerical simulation model and with field observations.

3.1. Discussion of Analytic Results

[31] We examine the dependences of n_i on w and T. One easily verifies that a_2 exceeds $a_3 S_{cr}$ by at least a factor of 3. Also, we recall that $\tau \propto w^{-1}$, $a_2 = n_{sat}^{-1}(T)$, and $b_1 \propto n_{sat}(S_{cr}-1)$, whereas a_1 and b_2 exhibit only weak dependences on T and none on S_{cr} or w. With this information we deduce the relationship

$$n_i \propto w^{3/2} n_{sat}^{-1/2}. \tag{13}$$

The ice crystal concentration does not depend explicitly on the nucleation rate J. The detailed form of J affects the onset of freezing but not the final number of crystals. In our solution, information about the freezing process is brought about by the freezing threshold saturation S_{cr} and the logarithmic derivative of J with respect to T through τ.

[32] The positive correlation between n_i and w shows that the higher the vertical velocity, the more ice particles form. This is because faster updrafts create higher supersaturations, allowing more particles to freeze before the supersaturation is depleted. Notably, this dependence is much greater than for cloud droplets nucleating on CCN, where the droplet concentration rises as $w^{(3/2)\,k/(k+2)}$, with typically $k \simeq 1/2$ (with an observed range $0.2 \leq k \leq 1$ for atmospheric CCNs), that is $\propto w^{3/10}$ [*Twomey*, 1977].

[33] The inverse exponential dependence of n_i on T (via n_{sat}) shows that the lower the temperature, the more particles freeze. This is because the growth rates decrease exponentially when T is lowered; the growing ice particles need longer to take up the available water vapor, allowing more ice particles to be formed.

[34] As we have seen in Figure 2, the fast-growth solution (equation (13)) is applicable to a wide range of values for T and w. If only large ($r_0 > 0.5$ μm) aerosol particles were present, this range would become narrower, and the slow-growth solution (equation (9a)) would be more appropriate, where n_i depends explicitly on r_0.

3.2. Parcel Model Simulations

3.2.1. Simulation model. [35] We compare the analytic relationships (equations (11a) and (12b)) for the number and mean size of cirrus ice particles with a large number of detailed numerical simulations. For this purpose, we employed the newly developed Advanced Particle Simulation Code (APSC), run in the adiabatic parcel mode with constant vertical velocity. Its microphysical part solves homogeneous freezing and size-resolved depositional growth of ice particles that form on multicomponent aerosol particles, in this case, on aqueous sulfuric acid aerosol. For the liquid solutions, we used the thermodynamical properties as described by *Kärcher et al.* [1998]. The physical processes are treated kinetically over a nondiffusive, moving center size structure. A noniterative, unconditionally stable, and mass-conserving treatment of condensation and nucleation, fully coupled to the gas phase, was applied [*Jacobson*, 1999]. The time steps range from 5 ms to 5 s, scaling inversely proportional to w, sufficiently small to yield accurate solutions. A coarse resolution of the aerosol size spectrum can lead to an incorrect calculation of the number of

ice crystals, for which reason we used 80 size bins and a bin volume ratio of 1.5 to discretize the aerosol properties. A detailed description of APSC will be published elsewhere (B. Kärcher, The Advanced Particle Simulation Code: Description and applications, manuscript in preparation, 2001).

[36] To ensure consistency with the results from section 2, we used the homogeneous nucleation rate developed by *Koop et al.* [2000]. The simulations started with a large reservoir of aerosol particles ($n > 1000$ cm^{-3}) at ice saturation at $p = 220$ hPa and at three selected temperatures (200, 220, and 240 K). We chose n to be always larger than n_i and chose updraft speeds ranging from 1 to 1000 cm s^{-1} to explore the full parameter range of the problem. The simulations were continued with constant w until the saturation ratio dropped and reached a quasi-steady state value (see right-hand side of Figure 1). Here the number density of crystals remains constant, and their size is approximately constant. (The ice crystals continue to grow slowly because the air remains slightly supersaturated, an effect not included in the theoretical model.).

[37] To evaluate (11a) and (12b), we started at the same conditions, located T and p when S_i became equal to S_{cr}, and computed n_i and r_i. Adiabatic changes in concentrations per unit volume of air were also considered in the analytic solution. In the APSC baseline simulations, aerosol particles were distributed lognormally, with a total mass of 1.2 μg m^{-3}, a mean mass radius of $r_m = 0.055$ μm, and a geometric width of $\sigma = 1.6$. The mass has been chosen such that the resulting number of aerosol particles, $n = 2500$ cm^{-3}, always exceeds the number of ice crystals that form from these aerosols. The mean radius and width were taken from airborne measurements in midlatitudes [*Schröder et al.*, 2001]. In addition, we ran cases with modified mean radius and width: a narrower size distribution with smaller particles ($r_m = 0.0275$ μm, $\sigma = 1.3$, and $n = 8600$ cm^{-3}) and a broader spectrum with larger particles ($r_m = 0.11$ μm, $\sigma = 2$, and $n = 2000$ cm^{-3}). These choices represent approximate bounds on accumulation-mode aerosol spectra. In the volcanically unperturbed atmosphere the variability of particles in this mode is likely to be smaller. In particular, the number of accumulation mode particles rarely exceeds 500 cm^{-3}.

3.2.2. Comparison with simulations. [38] We present the APSC results as symbols and the analytic results as solid curves in Figure 3. For each temperature, the upper/middle/lower symbols correspond to an initialization of narrower/baseline/broader aerosol size distributions; see section 3.2.1. We first discuss the numerical results. As all squares almost completely overlap, cirrus formation at the warmest temperature appears to be almost independent of details of the aerosol spectra over the entire range of w values. This also holds for intermediate temperatures (triangles) and for $w < 100$ cm s^{-1}. At the lowest temperature considered (circles), the sensitivity of n_i to aerosol properties becomes evident for $w > 10$ cm s^{-1}. However, deviations from the baseline results remain within a factor of 2 in most cases.

[39] This general insensitivity of the number of crystals formed to the aerosol physical properties is in excellent agreement with the basic physical assumptions of the theory as described in section 2. For our choice of parameters describing the accumulation mode and its extreme stages, a sensitivity can only be expected at the lowest temperatures in strong ascents, when nucleation almost instantaneously causes freezing of a large fraction of the available aerosol particles. In such cases, the initial size of the crystals decides whether growth takes place in the gas kinetic or diffusive regime; hence the dependence on r_0.

[40] The curves crossing the symbols at each temperatures demonstrate the quality of our analytic results. By constraining the single free model parameter $c(T)$ with (6d), the agreement with the APSC results is excellent in all cases not affected by the aerosol properties. In particular, the scaling of n_i with T and w (equation (13)) is perfectly reproduced. Since (11a) is only valid

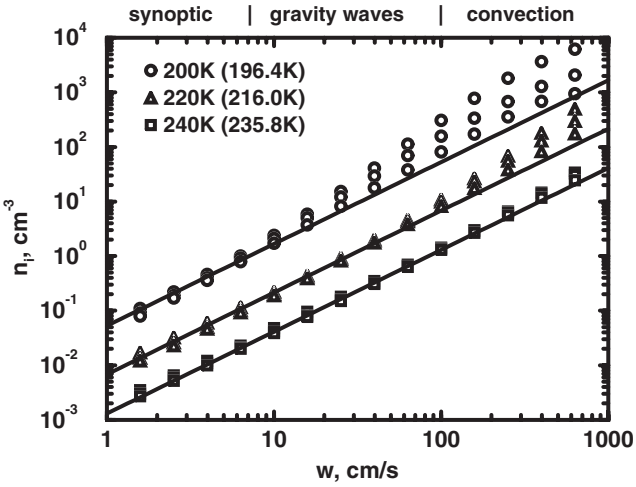

Figure 3. Cirrus ice crystal number densities as a function of vertical velocity at different temperatures from numerical simulations (symbols) and from the analytic solution (equation (11a)), supplemented by (6c) and (6d) (curves). Legend shows the frost point at which the air parcel starts rising from the 220 hPa level and the approximate temperature (value in brackets) at which freezing commences. At each temperature, middle symbols represent baseline aerosol runs and upper and lower symbols assume strongly perturbed aerosol properties. Physical mechanisms generating vertical motions in the atmosphere are indicated.

in the fast-growth regime, the agreement in the regions with high w and low T becomes poorer.

[41] While the analytic approach tends to underestimate n_i values at low T and high w as quantified above, we do not attempt to adjust the analytic solution, for three reasons. First, in many cases, the number of aerosol particles that freeze will be limited to values up to several hundred per cubic centimeter, where the slow-growth regime does not apply. Second, the low T and high w values for which the analytic solution becomes less accurate will occur much less frequently in the atmosphere than the most typical values (T around 220 K and w in the gravity wave regime of several tens of centimeters per second). Third, it is desirable to keep the analytic solution as simple as possible because it should also be applicable in a climate model).

[42] To complete this discussion, we compare our analytic results (as discussed in Figure 3) from (11a) to the parameterization presented by *Sassen and Benson* [2000], $n_i^{SB} = a(w) \exp[b(w)T]$. The coefficients a and b are second-order polynomials in w fitted to numerical parcel simulation results in the updraft range $4 < w$ [cm s^{-1}] < 100 using a molality-based, effective freezing temperature of ammonium sulfate aerosols. The dependence on S_{cr}, which is a function of T and w in this approach, is implicitly contained in n_i^{SB}.

[43] Both parameterizations predict a marked increase of n_i with rising w and a decrease of n_i with rising T. While the overall agreement is fair around 200 K, the scheme of *Sassen and Benson* [2000] yields progressively higher crystal number densities at higher temperatures. The reason for these deviations is not fully clear and could be tied to the different treatment of the freezing threshold or aerosol properties or to numerical issues. The polynomials generate an oscillatory behavior in n_i^{SB} that has no obvious physical explanation according to the mechanisms underlying cirrus formation as detailed in section 2 and could be an artifact of the fit functions used to constrain the coefficients a and b.

3.2.3. Comparison with observations. [44] A detailed comparison of the results shown in Figure 3 with cirrus measurements is difficult, because the exact vertical velocities

and aerosol parameters at the time of ice formation are usually not known. Also, very few in situ data are available that were taken in ice clouds that form in slowly rising air parcels, but those would be the best choice for a comparison with the present parameterization.

[45] We find a very good general agreement with the airborne measurements taken by *Ström et al.* [1997], who reported ambient crystal number densities of the order of 0.3 cm^{-3} at the top of a young cirrus cloud formed at 8.8 km and 220 K, presumably by homogeneous freezing. (The observed relative humidity there was near water saturation.) During this measurement the standard deviation of w around a mean value near zero was $\sim$20 cm s^{-1}, averaging horizontal scales between 0.5 and 10 km, which indicates gravity wave activity. Under these conditions at a freezing temperature of 220 K, our analytic model predicts n_i = 0.18 (0.5) cm^{-3} at w = 10 (20) cm s^{-1}.

[46] We compare our results with observations in wave clouds reported by *Jensen et al.* [1998]. Two data sets are discussed by these authors: a cirrus formed near 12 km altitude around 209 K at w = 0.8–1.6 m s^{-1} with peak n_i values of 2–7 cm^{-3} (cold case) and a cirrus formed near 9 km around 237 K at w = 3–5 m s^{-1} with n_i = 20–40 cm^{-3} (warm case). Using these data, we compute n_i = 8–24 cm^{-3} in the cold case and n_i = 9–20 cm^{-3} in the warm case. The agreement is satisfactory, given the uncertainties of the reported conditions at the time of cloud formation; also, because of the relatively high updraft speeds, aerosol size effects could have played a larger role in determining n_i as compared to the *Ström et al.*1997 data set.

4. Aspects of Large-Scale Model Applications

4.1. Model Time Steps and Ice Supersaturation

[47] Typical model time steps Δt of GCMs range from 10 to 40 min. Starting from a given ice saturation ratio S_0 and updraft speed w, S_i must surpass the freezing threshold S_{cr} for cloud formation to occur within Δt. Once ice crystals have formed, equilibrium with respect to ice may not be reached within Δt when growth rates are too slow. These two facts underscore the need to allow for ice supersaturation to occur in GCMs. We discuss them subsequently.

[48] In principle, S_i can have any value in a given grid box at the beginning of a new time step. Using (1), the time t_{cr} needed to reach S_{cr} starting from S_0 (see Figure 1) is approximately given by

$$t_{cr} = \frac{1}{a_1 w} \ln\left(\frac{S_{cr}}{S_0}\right); \qquad (14)$$

the factor $a_1 \simeq 10^{-5}$ cm^{-1} depends weakly on temperature. For instance, $t_{cr} \simeq 35$ min for $w \simeq 20$ cm s^{-1}. If ice supersaturation is allowed to occur, we eventually start from a value S_0 below but close to S_{cr} so that the cloud forms within the next time step. As a consequence, varying Δt will slightly shift the onset of cloud formation in time.

[49] Concerning freezing, we assume that n_i from (11a), the mean radius (equation (11b)) and ice water mass (equation (11c)) at the time where S_i reaches a peak are achieved instantaneously as compared to Δt. Concerning growth, however, it will take a longer time until m_i and r_i reach their final values (equations (12a) and (12b)) after S_i relaxes to unity. It may happen that these equilibrium values are not reached within Δt. The equilibrium radii (solid curves) and corresponding ice water masses (dashed lines) are shown in Figure 4, computed with the crystal number densities as plotted in Figure 3. In our approach, the final ice water mass does not depend on w but scales in proportion to the H_2O saturation number density at the freezing temperature and the peak supersaturation achieved in the air parcel and ranges from 0.65 mg m^{-3} at 200 K to 70 mg m^{-3} at 240 K.

[50] To illustrate the growth timescales in young cirrus clouds, Figure 5 shows the times needed to grow ice particles to 80% of their mean final sizes (see Figure 4) as a function of temperature.

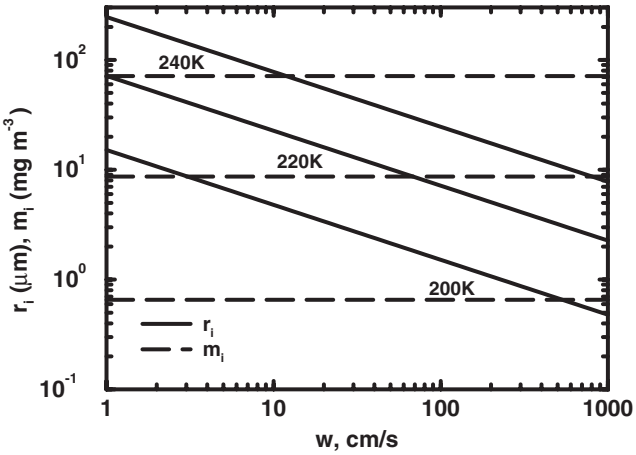

Figure 4. Mean ice crystal radii (solid curves) and ice water masses (dashed lines) after complete relaxation from the analytic solution (equation (12b)) versus vertical velocity for different temperatures, corresponding to the crystal number densities shown in Figure 3.

The labels on the curves indicate the number densities of ice particles. Initial conditions are noted in the caption. We obtained these results by integrating the growth equation (equation (7)) along with the conservation of H_2O [*Kärcher and Solomon*, 1999], resulting in the solution

$$t(x)/t_g = (\beta+1)[\mathcal{I}_1(x) - \mathcal{I}_1(x_0)] + (\beta-1)[\mathcal{I}_2(x) - \mathcal{I}_2(x_0)], \qquad (15)$$

where $\beta = 4D/(v_{th}\,\alpha r_i)$, $t_g = 3/(4\pi n_i D r_i)$, $x_0 = r_0/r_i$, $x_0 \le x = R/r_i \le 1$, and

$$\mathcal{I}_1(x) = \frac{1}{6} ln\left[\frac{1+x+x^2}{(1-x)^2}\right],$$

$$\mathcal{I}_2(x) = \frac{1}{\sqrt{3}} \arctan\left(\frac{1+2x}{\sqrt{3}}\right).$$

(At this point, we correct a typo in the work of *Kärcher and Solomon* [1999], equation (B9), p. 27,456. Equation (15) is the correct expression for the scaled growth time t/t_g.)

[51] Figure 5 reveals that for T = 220 K, growth times are smaller than $\sim$20 min for $n_i > 0.1$ cm^{-3}, or, using Figure 3, for $w > 10$ cm s^{-1}. At lower temperatures or weaker updrafts, growth times can become quite long (many hours). These particles grow sufficiently large to cause rapid gravitational settling of the ice particles, implying that clouds that form under such conditions will never reach an equilibrium state. For $T < 200$ K, the growth times become very short in strong updrafts: because of the small mass of available water vapor, the mean final crystal size only slightly exceeds the assumed initial size when ice particle concentrations exceed $\sim$100 cm^{-3}.

[52] To estimate the expected departure of r_i (and m_i) from their equilibrium values due to a finite model time step, we compute $r_i(\Delta t)$ by inverting (15) with $t(x) = \Delta t$ and $x_0 = r_{i*}/r_i$ using (11b). We find that once freezing occurs, growth is often rapid enough to allow for relaxation of S_i within Δt; see Figure 5.

[53] In most current GCMs with explicit cirrus cloud microphysics, gaseous H_2O in excess of ice saturation is moved to cloud ice, preventing ice supersaturations from ever occurring. We propose to remove this constraint in order to obtain a more realistic description of cirrus formation. Dropping the saturation adjustment likely involves further model tuning to reproduce realistic relative

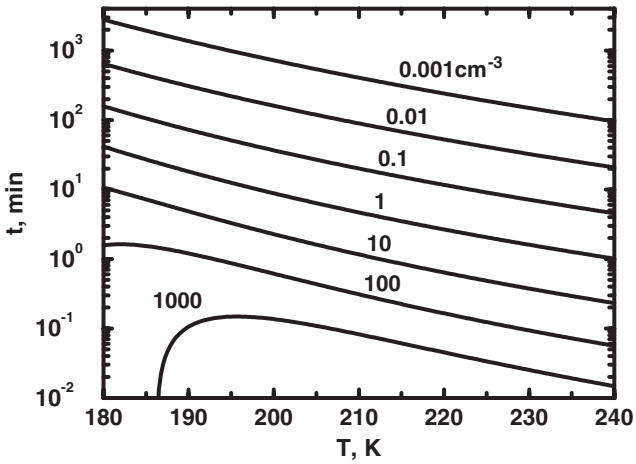

Figure 5. Time for spherical, monodisperse ice particles to grow to 80% of their equilibrium radius versus temperature. Constant number density of ice particles is given for each curve. Calculations were performed using the analytic solution for ice particle growth from *Kärcher and Solomon* [1999] and assume an air pressure of 200 hPa, an initial ice saturation ratio of 1.3, an initial particle radius of 0.25 μm, and a deposition coefficient of H_2O molecules onto ice of 0.5.

humidity fields. However, climatological information on upper tropospheric humidity is not available, except for selected atmospheric regions regularly probed by commercial aircraft [*Gierens et al.*, 1999].

4.2. Subgrid-Scale Variability of Vertical Motions

[54] According to observations, cirrus occurrence becomes more likely as the vertical motion increases. Cirrus may exist, but are unlikely to form, in regions with descending air [e.g., *Ström et al.*, 1997]. It is important to note that for our purposes, the vertical velocity w used in our parameterization to compute the initial cloud properties is the velocity at the scale of cloud formation. Unfortunately, the present knowledge on upper tropospheric vertical velocities and the vertical motion variability is poor, partly because updrafts are not easily measured in situ and systematic studies with an extended spatial coverage are not available.

[55] The variance σ_w of w depends on the averaging horizontal scale ℓ, ranging from $\sigma_w = 5-20$ cm s^{-1} for $\ell = 100-1$ km [*Ström et al.*, 1997]. Since such scales are not resolved by current GCMs, the model grid mean vertical speeds $\overline{w}$ must be corrected at least by an estimate of the mean fluctuations Δw such that $w = \overline{w} + \Delta w$.

[56] Equation (13) predicts that $n_i \propto w^{3/2}$. Using this scaling we derive

$$\frac{n_i(w)}{n_i(\overline{w})} = k \rightarrow \frac{\Delta w}{\overline{w}} = k^{2/3} - 1. \qquad (16)$$

In the European Center for Medium Range Weather Forecast model Hamburg version (ECHAM) GCM, for example, *Lohmann et al.* [1999] estimated the variances Δw used in the cloud droplet activation scheme by $0.7\sqrt{\mathrm{TKE}}$, where TKE is the turbulent kinetic energy. For cloudy grid boxes at $T < 235$ K located in the upper troposphere, we find vertical velocities ranging between 1 and 3440 cm s^{-1}, with a mean value $\overline{w} = 2.8$ cm s^{-1} and $\Delta w/\overline{w} = 14$. Using the above relationships, we compute $k = 58$ and thus $n_i(w) = 58 n_i(\overline{w})$. This simple estimate underscores the need to include the variability of w in the prediction of cirrus properties.

5. Role of Aerosol Size Effects and Heterogeneous Freezing

5.1. Effects of Aerosol Size

[57] We found that the number of ice crystals formed homogeneously in cirrus is rather insensitive to the aerosol size distribution. This implies that moderate anthropogenic changes of the number and size of liquid aerosol particles, for instance through the sulfate cycle, will only cause weak changes of the cirrus cloud properties that would hardly become observable. The homogeneous freezing data employed in this work imply that changes of the chemical composition of aerosols will not influence the freezing properties as long as the cirrus nuclei are liquid solution droplets.

[58] Aerosol size effects can become important in two cases: (1) when a sufficient number of large particles (>0.5–1 μm) are present that freeze earlier by homogeneous nucleation than those from the accumulation mode used in this work, and (2) if the entire aerosol freezes heterogeneously at relative humidities well below the homogeneous threshold ($S_{cr} \ll 1.4$). In both cases, κ from (kappa) decreases at any fixed values of T and w, and we can expect deviations from the parameterization; see also section 3.1. In upper tropospheric cirrus, larger haze mode particles are known to exist [e.g., *Schröder et al.*, 2000] but are difficult to quantify in terms of size distribution and chemical composition. Evidence for an aerosol size effect is found under volcanically perturbed conditions [*Sassen*, 1992], where many very large particles that formed in the lower stratosphere are transported into the upper troposphere by sedimentation and tropopause foldings. However, the freezing mode of the volcanic particles remains unclear.

[59] In summary, the atmospheric variability of w and T causes a large spread in cirrus properties, as n_i exhibits a marked dependence on these parameters. We may argue that this variability alone could explain a large part of the huge variance of cirrus properties [e.g., *Dowling and Radke*, 1990]. However, a definite conclusion on this point can only be drawn theoretically when aerosol effects are included in the parameterization.

5.2. Potential Effects of Heterogeneous Freezing Nuclei

[60] Cirrus may also form heterogeneously in the presence of suitable ice nucleating aerosols that form ice at lower humidities than required for homogeneous freezing. Natural FN in the upper troposphere contain crustal and carbonaceous material. Freezing nuclei originating from anthropogenic emissions include mixed soot/sulfate and metallic particles [*Heintzenberg et al.*, 1996; *Chen et al.*, 1998].

[61] The effects of efficient FN may cause significant changes of the cloud properties [e.g., *DeMott et al.*, 1998; *Spice et al.*, 1999]. In mixtures of particles with different freezing thresholds, different parts of the aerosol spectrum can compete for the available water vapor so that even very few (0.01 cm^{-3}) effective FN may control the freezing and growth dynamics [*Jensen et al.*, 2001]. This competition becomes especially relevant in slow updrafts, where the number of homogeneously nucleated ice particles remain small and comparable to the number of efficient FN.

[62] We finally add that for almost perfect FN with $S_{cr} \rightarrow 1$, κ approaches zero for all values T and w. In such cases, (11a) cannot be applied, and we have to use the slow-growth solution, which contains the aerosol size r_0 as a further parameter. For FN with S_{cr} values between 1 and 1.4, fast- and slow-growth solutions must be combined to achieve a proper parameterization. (Of course, this is feasible only for heterogeneous freezing modes that can be treated within the present theoretical model framework.) We expect a marked sensitivity of cirrus formation on the relative concentration, size, and mixing state of the particles with different freezing thresholds, just as it is the case for a mixture of chemically different CCNs in liquid clouds.

6. Summary and Outlook

[63] We have developed a physically based parameterization of cirrus cloud formation by homogeneous freezing of aerosols. Our parameterization applies to a wide class of aqueous solutions relevant to homogeneous freezing in the atmosphere, because the freezing thresholds on which the model is based have been shown to be determined by temperature and water activity (i.e., relative humidity) alone, independent of the chemical nature of the particles.

[64] We have explored the physical processes involved in the formation of cold cirrus and have highlighted problems that arise when the parameterization is utilized in a large-scale atmospheric model. We have discussed the role of aerosol size effects and the presence of heterogeneous freezing nuclei on the cloud initiation process.

[65] We regard this work as the first step of a systematic development of a theoretical model framework that eventually also includes heterogeneous freezing processes. The main results of our study are as follows:

1. For supercooled liquid aerosol particles the number of ice crystals formed by homogeneous freezing is controlled by the vertical velocity and the temperature of the air parcel rather than by details of the aerosol size distribution. The number of crystals formed in this way increases with increasing vertical velocity and decreasing temperature.
2. In large-scale atmospheric models with explicit cloud microphysics, supersaturations with respect to ice must be allowed in order to obtain a more realistic calculation of cirrus formation in the upper troposphere. It is important to include the subgrid-scale variability of vertical motions in global models in estimating the initial number, size, and mass of cirrus ice crystals.
3. The atmospheric variability of vertical motion and temperature, and changes thereof caused by natural and anthropogenic processes, is expected to cause a large spread of cirrus properties. In comparison, it is likely that for pure homogeneous freezing, anthropogenic changes of the volatile aerosol chemical composition (e.g., of the abundance of sulfates) exert only a weak impact on cirrus cloud properties.

[66] The approximate insensitivity of the initial cloud parameters to the properties of the aerosol size distribution is very convenient in terms of employing the parameterization in a GCM, since most current climate models do not carry aerosol parameters such as number and size explicitly. We plan to use it in the global climate model ECHAM as a first step to investigate the link between aerosols and cirrus clouds by interactively coupling high-cloud properties with atmospheric dynamics and radiation. The parameterization can also be applied in cloud-resolving simulation models, which usually have a more realistic representation of the vertical wind field than GCMs.

[67] Moreover, it will be useful to extend our parameterization by combining the limiting cases for slow and fast ice particle growth. This will enable us to treat homogeneous freezing of multimodal aerosol distributions of arbitrary size and shape as well as to contrast homogeneous and heterogeneous freezing mechanisms in future work on cirrus parameterizations. Inclusion of heterogeneous processes in our model framework may not be possible for all existing modes of action of ice-forming particles. These extensions would call for the need to include size-segregated aerosol information in global models. First steps are underway to couple multimodal aerosol dynamics to atmospheric transport processes [*Raes et al.*, 2000]. Such coupled models permit a more realistic treatment of aerosol-cloud and aerosol-chemistry processes in future simulations of climate.

[68] With regard to future experimental work, two main avenues of research are emanating: continuation of efforts to experimentally determine relationships between aerosol and cloud properties and identification of the origin, nature, and properties of upper tropospheric freezing nuclei.

Notation

a_k, b_k coefficients in (1) and (7).
α deposition coefficient of water molecules on ice.
c fit parameter in (6c).
κ dimensionless parameter in (10).
m_i ice water mass.
m_w mass of a water molecule.
n total number density of aerosol particles.
n_i total number density of ice particles.
n_{sat} saturation vapor number density over ice.
p pressure.
r_i ice particle radius.
r_0 aerosol or ice particle radius at time t_0.
R_i freezing/growth integral in (2a).
ρ_i mass density of ice particles.
S_i saturation ratio over a plane ice surface in (1).
S_{i*} peak saturation ratio.
S_{cr} freezing threshold saturation ratio.
t time.
t_0 time when freezing commences.
T temperature.
τ freezing timescale.
v_{th} thermal speed of water molecules.
w vertical velocity.
$*$ subscript indicating values at the time when $S_i = S_{i*}$.
0 superscript for the slow-growth regime.
∞ superscript for the fast-growth regime.

[69] **Acknowledgments.** We would like to thank Ian Ford for fruitful discussions on the solution strategy. This research contributed to the HGF/BMBF project "Particles and Cirrus Clouds" and was supported by the National Science and Engineering Research Council of Canada.

References

Abdul-Razzak, H., S. J. Ghan, and C. Rivera-Carpio, A parameterization of aerosol activation, I, Single aerosol type, *J. Geophys. Res.*, *103*, 6123–6132, 1998.

Albrecht, B. A., Aerosols, cloud microphysics, and fractional cloudiness, *Science*, *245*, 1227–1230, 1989.

Boucher, O., and U. Lohmann, The sulfate–CCN–cloud albedo effect: A sensitivity study with two general circulation models, *Tellus, Ser. B*, *47*, 281–300, 1995.

Charlson, R. J., and J. Heintzenberg (Eds.), *Aerosol Forcing of Climate: Report of the Dahlem Workshop on Aerosol Forcing of Climate, Berlin 1994, April 24–29*, John Wiley, New York, 1995.

Charlson, R. J., J. E. Lovelock, M. O. Andreae, and S. G. Warren, Oceanic phytoplankton, atmospheric sulfur, cloud albedo and climate, *Nature*, *326*, 655–661, 1987.

Chen, Y., S. M. Kreidenweis, L. M. McInnes, D. C. Rogers, and P. J. DeMott, Single particle analyses of ice-nucleating aerosols in the upper troposphere and lower stratosphere, *Geophys. Res. Lett.*, *25*, 1391–1394, 1998.

Del Genio, A. D., M. S. Yao, W. Kovari, and K. K. W. Lo, A prognostic cloud water parameterization for global climate models, *J. Clim.*, *9*, 270–304, 1996.

DeMott, P. J., D. C. Rogers, and S. M. Kreidenweis, The susceptibility of ice formation in upper tropospheric clouds to insoluble aerosol components, *J. Geophys. Res.*, *102*, 19,575–19,584, 1997.

DeMott, P. J., D. C. Rogers, S. M. Kreidenweis, Y. Chen, C. H. Twohy, D. Baumgardner, A. J. Heymsfield, and K. R. Chan, The role of heterogeneous freezing nucleation in upper tropospheric clouds: Inferences from SUCCESS, *Geophys. Res. Lett.*, *25*, 1387–1390, 1998.

DeMott, P. J., Y. Chen, S. M. Kreidenweis, D. C. Rogers, and D. E. Sherman, Ice formation by black carbon particles, *Geophys. Res. Lett.*, *26*, 2429–2432, 1999.

Dowling, D. R., and L. F. Radke, A summary of the physical properties of cirrus clouds, *J. Appl. Meteorol.*, *29*, 970–978, 1990.

Ford, I., How aircraft nucleate ice particles: A simple model, *J. Aerosol Sci.*, *29*, S1117, 1998.

Fowler, L. D., D. A. Randall, and S. A. Rutledge, Liquid and ice cloud microphysics in the CSU general circulation model, I, Model description and simulated microphysical processes, *J. Clim.*, *9*, 489–529, 1996.

Ghan, S. J., L. R. Leung, R. C. Easter, and H. Abdul-Razzak, Prediction of cloud droplet number in a general circulation model, *J. Geophys. Res.*, *102*, 21,777–21,794, 1997.

Gierens, K. M., U. Schumann, M. Helten, H. Smit, and A. Marenco, A distribution law for relative humidity in the upper troposphere and lower stratosphere derived from three years of MOZAIC measurements, *Ann. Geophys.*, *17*, 1218–1226, 1999.

Hanson, D., and K. Mauersberger, Laboratory studies of the nitric acid trihydrate: Implications for the South Polar stratosphere, *Geophys. Res. Lett.*, *15*, 855–858, 1988.

Heintzenberg, J., K. Okada, and J. Ström, On the composition of nonvolatile material in upper tropospheric aerosols and cirrus ice crystals, *Atmos. Res.*, *41*, 81–88, 1996.

Heymsfield, A. J., and L. M. Miloshevich, Relative humidity and temperature influences on cirrus formation and evolution: Observations from wave clouds and FIRE-II, *J. Atmos. Sci.*, *52*, 4302–4326, 1995.

Heymsfield, A. J., and R. M. Sabin, Cirrus crystal nucleation by homogeneous freezing of solution droplets, *J. Atmos. Sci.*, *46*, 2252–2264, 1989.

Intergovernmental Panel on Climate Change (IPCC), *Climate Change 2001: The Science of Climate Change*, Third Assessment Report, edited by J. T. Houghton, et al., 944 pp., Cambridge Univ. Press, New York, 2001.

Jacobson, M. Z., *Fundamentals of Atmospheric Modeling*, 656 pp., Cambridge Univ. Press, New York, 1999.

Jensen, E. J., et al., Ice nucleation processes in upper tropospheric wave-clouds observed during SUCCESS, *Geophys. Res. Lett.*, *25*, 1363–1366, 1998.

Jensen, E. J., O. B. Toon, S. A. Vay, J. Ovarlez, R. May, P. Bui, C. H. Twohy, B. Gandrud, R. F. Pueschel, and U. Schumann, Prevalence of ice-supersaturated regions in the upper troposphere: Implications for optically thin ice cloud formation, *J. Geophys. Res.*, *106*, 17,253–17,266, 2001.

Kärcher, B., and S. Solomon, On the composition and optical extinction of particles in the tropopause region, *J. Geophys. Res.*, *104*, 27,441–27,459, 1999.

Kärcher, B., R. Busen, A. Petzold, F. P. Schröder, U. Schumann, and E. J. Jensen, Physicochemistry of aircraft generated liquid aerosols, soot, and ice particles, 2, Comparison with observations and sensitivity studies, *J. Geophys. Res.*, *103*, 17,129–17,148, 1998.

Khvorostyanov, V., and K. Sassen, Toward the theory of homogeneous nucleation and its parameterization for cloud models, *Geophys. Res. Lett.*, *25*, 3155–3158, 1998.

Koop, T., B. P. Luo, A. Tsias, and T. Peter, Water activity as the determinant for homogeneous ice nucleation in aqueous solutions, *Nature*, *406*, 611–614, 2000.

Liou, K.-N., Influence of cirrus clouds on weather and climate processes: A global perspective, *Mon. Weather Rev.*, *114*, 1167–1199, 1986.

Lohmann, U., Possible aerosol effects on ice clouds via contact nucleation, *J. Atmos. Sci.*, in press, 2001.

Lohmann, U., J. Feichter, C. C. Chuang, and J. E. Penner, Predicting the number of cloud droplets in the ECHAM GCM, *J. Geophys. Res.*, *104*, 9169–9198, 1999.

Lohmann, U., J. Feichter, J. E. Penner, and W. R. Leaitch, Indirect effect of sulfate and carbonaceous aerosols: A mechanistic treatment, *J. Geophys. Res.*, *105*, 12,193–12,206, 2000.

Newell, R. E., Y. Zhu, E. V. Browell, S. Ismail, W. G. Read, J. W. Waters, K. K. Kelly, and S. C. Liu, Upper tropospheric water vapor and cirrus: Comparison of DC-8 observations, preliminary UARS Microwave Limb Sounder measurements, and meteorological analyses, *J. Geophys. Res.*, *101*, 1931–1941, 1996.

Pruppacher, H. R., and J. D. Klett, *Microphysics of Clouds and Precipitation*, Kluwer Acad., Norwell, Mass., 1997.

Raes, F., R. Van Dingenen, E. Vignati, J. Wilson, J.-P. Putaud, J. H. Seinfeld, and P. Adams, Formation and cycling of aerosols in the global troposphere, *Atmos. Environ.*, *34*, 4215–4240, 2000.

Rotstayn, L. D., Indirect forcing by anthropogenic aerosols: A global climate model calculation of the effective radius and cloud lifetime effects, *J. Geophys. Res.*, *104*, 9369–9380, 1999.

Sassen, K., Evidence for liquid-phase cirrus cloud formation from volcanic aerosols: Climatic implications, *Science*, *257*, 516–519, 1992.

Sassen, K., and G. C. Dodd, Haze particle nucleation simulation in cirrus clouds and application for numerical and lidar studies, *J. Appl. Sci.*, *46*, 3005–3014, 1989.

Sassen, K., and S. Benson, Ice nucleation in cirrus clouds: A model study of the homogeneous and heterogeneous modes, *Geophys. Res. Lett.*, *27*, 521–524, 2000.

Schröder, F., B. Kärcher, C. Duroure, J. Ström, A. Petzold, J.-F. Gayet, B. Strauss, P. Wendling, and S. Borrmann, On the transition of contrails into cirrus clouds, *J. Atmos. Sci.*, *57*, 464–480, 2000.

Schröder, F., B. Kärcher, A. Petzold, and M. Fiebig, Aerosol sources and transformation processes in the free troposphere and tropopause region at northern midlatitudes, *J. Geophys. Res.*, in press, 2002.

Schumann, U., H. Schlager, F. Arnold, J. Ovarlez, H. Kelder, Ø. Hov, G. Hayman, I. S. A. Isaksen, J. Staehelin, and P. D. Whitefield, Pollution from aircraft emissions in the North Atlantic flight corridor: Overview on the POLINAT projects, *J. Geophys. Res.*, *105*, 3605–3631, 2000.

Spice, A., D. W. Johnson, P. R. A. Brown, A. G. Darlison, and C. P. R. Saunders, Primary ice nucleation in orographic cirrus clouds: A numerical simulation of the microphysics, *Q. J. R. Meteorol. Soc.*, *125*, 1637–1667, 1999.

Ström, J., and S. Ohlsson, In situ measurements of enhanced crystal number densities in cirrus clouds caused by aircraft exhaust, *J. Geophys. Res.*, *103*, 11,355–11,361, 1998.

Ström, J., B. Strauss, T. Anderson, F. Schröder, J. Heintzenberg, and P. Wendling, In situ observations of the microphysical properties of young cirrus clouds, *J. Atmos. Sci.*, *54*, 2542–2553, 1997.

Tabazadeh, A., S. T. Martin, and J.-S. Lin, The effect of particle size and nitric acid uptake on the homogeneous freezing of aqueous sulfuric acid particles, *Geophys. Res. Lett.*, *27*, 1111–1114, 2000.

Twomey, S., The nuclei of natural cloud formation, II, The supersaturation in natural clouds and variation of cloud droplet concentration, *Geofis. Pura Appl.*, *43*, 243–249, 1959.

Twomey, S., *Atmospheric Aerosols*, *Dev. in Atmos. Sci.*, vol. 7, North-Holland, New York, 1977.

Twomey, S., Aerosols, clouds, and radiation, *Atmos. Environ., Part A*, *25*, 2435–2442, 1992.

Wilson, D. R., and S. P. Ballard, A microphysically based precipitation scheme for the UK Meteorological Office Unified Model, *Q. J. R. Meteorol. Soc.*, *125*, 1607–1636, 1999.

B. Kärcher, DLR Oberpfaffenhofen, Institut für Physik der Atmosphäre, D-82 Postfach 1116, Oberpfaffenhofen, 234 Wessling, Germany. (bernd.kaercher@dlr.de)

U. Lohmann, Atmospheric Science Program, Department of Physics, Dalhousie University, Halifax, Nova Scotia, B3H 3J5, Canada. (Ulrike. Lohmann@Dal.Ca)